

Radio Emission from Interstellar Shocks: Young Type Ia Supernova Remnants and the Case of N 103B in the Large Magellanic Cloud

Alsaberi R. Z. E.¹ • Barnes L. A.¹ •
 Filipović M. D.¹ • Maxted N. I.^{1,2} • Sano H.³ •
 Rowell G.⁴ • Bozzetto L. M.¹ • Gurovich S.⁵ •
 Urošević D.⁶ • Onić D.⁶ • For B.-Q.⁷ •
 Manojlović P.^{1,8} • Wong G.¹ • Galvin T.^{1,8} •
 Kavanagh P.⁹ • Ralph N.¹ • Crawford E. J.¹ •
 Sasaki M.¹⁰ • Haberl F.¹¹ • Maggi P.¹² •
 Tothil N. F. H.¹ • Fukui Y.³

Abstract

Alsaberi R. Z. E.
 Barnes L. A.
 Filipović M. D.
 Maxted N. I.
 Sano H.
 Rowell G.
 Bozzetto L. M.
 Gurovich S.
 Urošević D.
 Onić D.
 For B.-Q.
 Manojlović P.
 Wong G.
 Galvin T.
 Kavanagh P.
 Ralph N.
 Crawford E. J.
 Sasaki M.
 Haberl F.
 Maggi P.
 Tothil N. F. H.
 Fukui Y.

¹Western Sydney University, Locked Bag 1797, Penrith South DC, NSW 1797, Australia

²School of Science, University of New South Wales, Australian Defence Force Academy, Canberra, ACT 2600, Australia

³Institute for Advanced Research, Nagoya University, Chikusa-ku, Nagoya 464-8601, Japan

⁴School of Physical Sciences, University of Adelaide, North Terrace, Adelaide, SA 5005, Australia

⁵Instituto de Astronomía Teórica y Experimental - Observatorio Astronómico Córdoba (IATE-OAC-UNC-CONICET)

⁶Department of Astronomy, Faculty of Mathematics, University of Belgrade, Studentski trg 16, 11000 Belgrade, Serbia

⁷International Centre for Radio Astronomy Research, University of Western Australia, 35 Stirling Hwy, Crawley, WA 6009,

We investigate young type Ia supernova remnants (SNRs) in our Galaxy and neighbouring galaxies in order to understand their properties and early stage of their evolution. Here we present a radio continuum study based on new and archival data from the Australia Telescope Compact Array (ATCA) towards N 103B, a young (≤ 1000 yrs) spectroscopically confirmed type Ia SNR in the Large Magellanic Cloud (LMC) and proposed to have originated from a single degenerate (SD) progenitor. The radio morphology of this SNR is asymmetrical with two bright regions towards the north-west and south-west of the central location as defined by radio emission.

N 103B identified features include: a radio spectral index of -0.75 ± 0.01 (consistent with other young type Ia SNRs in the Galaxy); a bulk SNR expansion rate as in X-rays; morphology and polarized electrical field vector measurements where we note radial polarisation peak towards the north-west of the remnant at both 5500 and 9000 MHz. The spectrum is concave-up and the most likely reason is the non-linear diffusive shock acceleration (NLDSA) effects or presence of two different populations of ultra-relativistic electrons.

We also note unpolarized clumps near the south-west region which is in agreement with this above scenario. We derive a typical magnetic field strength for N 103B of $16.4 \mu\text{G}$ for an average rotation measurement of 200 rad m^{-2} . However, we estimate the equipartition field to be of the order of $\sim 235 \mu\text{G}$ with an estimated minimum energy of $E_{\min} = 6.3 \times 10^{48} \text{ erg}$. The close ($\sim 0.5^\circ$) proximity of N 103B to the LMC mid-plane indicates that an early encounter with dense interstellar medium may have set an important constraint on SNR evolution.

Australia. ARC Centre of Excellence for All Sky Astrophysics in 3 Dimensions (ASTRO 3D)

Finally, we compare features of N 103B to six other young type Ia SNRs in the LMC and Galaxy, with a range of proposed degeneracy scenarios to highlight potential differences due to a different models. We suggest that the single degenerate scenario might point to morphologically asymmetric type Ia supernova explosions.

Keywords ISM: individual objects: N 103B, ISM: supernova remnants, radio continuum: ISM, supernovae: general

1 Introduction

Supernovae (SNe) play important roles in cosmology. Type Ia SNe have been used as standard candles to constrain cosmological parameters, providing the first and best evidence of cosmic acceleration and dark energy (Riess et al. 1998; Perlmutter et al. 1999). Further, SNe shape the way that galaxies form and evolve. SNe distribute the products of stellar nucleosynthesis into the interstellar medium (ISM), enriching, heating and compressing gas that forms second and third generation stars. The combined effect of many SN explosions in star-forming galaxies can drive gas out of galaxies and into the circum- and intergalactic medium. Observations of high-redshift star-forming galaxies have shown abundant evidence of galactic-scale outflows; as Steidel et al. (2010) and Nuza et al. (2019) have noted, virtually every $z > 2$ galaxy bright enough to be observed spectroscopically is driving out material at several hundred kilometers per second.

As a result, observations of SNe in the local/nearby Universe can inform both the measurement of cosmological parameters and theoretical models of galaxy formation. Data from nearby SNe and supernova remnants (SNRs) via systematic monitoring campaigns are particularly useful since many of these systems offer time-domain data that are costly to obtain or not possible at higher redshift.

In particular, nearby Universe observations have the potential for understanding the causes of SNe, assuming that the explosion mechanisms do not significantly change over cosmic time. Type Ia SNe (a.k.a. thermonuclear (TN)) are believed to occur when a white dwarf (WD) close to the Chandrasekhar mass, reigniting explosive nuclear reactions. This is most likely to occur in a binary system, either by the accretion from a non-degenerate companion star (the so-called single degenerate scenario, SD) or via a merger with another WD (double degenerate scenario, DD). Core collapse SNe (CC; SN II, SN Ib and SN Ic) result from the collapse of a single short lived massive star ($> 8M_{\odot}$) as it

exhausts its nuclear fuel. Intriguingly, the ratio of SN Ia to CC explosions is lower in large disk galaxies (like the Milky Way) than in dwarf irregular galaxies, implying that Galactic environment and different star formation rate (SFR) cannot be ignored (Tsujimoto et al. 1995). This effect is been shown by the recent observational evidence from nearby dwarfs–Magellanic Clouds (see Maggi et al. 2016).

A major remaining unknown is the proportion of type Ia SNe that result from the SD and DD scenarios (see e.g. Nomoto and Kondo 1991; Fryer et al. 2010). The decisive signature of an SD explosion is the observation of the surviving companion star, because the merger of the two WDs in the DD scenario leaves no remnant star. Other signatures include a dense circumstellar medium (Douvion et al. 2001; Blair et al. 2007; Williams et al. 2012), accretion winds from the progenitor system (Hachisu et al. 1996; Sano et al. 2018), and strong K-shell emission from Ni and Mn (Yamaguchi et al. 2015). Detailed observations of type Ia SNRs, to reconstruct the scene of the explosion and pinpoint the likely location of a surviving companion (if it exists), are required to distinguish between the SN scenarios. There may be other ways in which SNR indicate the scenario of their creation (Chakraborti et al. 2016).

Studies of SNRs in the Milky Way suffer from imprecise distance measurements and foreground absorption from the Galactic plane. Many of these problems are largely overcome by studying SNRs in the Large Magellanic Cloud (LMC). The LMC, with an distance of ~ 50 kpc (Macri et al. 2006; Pietrzyński et al. 2019) and a near face on orientation (inclination angle of 35°), is near enough to allow deep, high-resolution, multi-frequency observations (Maggi et al. 2016; Bozzetto et al. 2017). The LMC has active star-forming regions, and is located outside of the Galactic plane where absorption by gas and dust is reasonably low. The Small Magellanic Cloud (SMC), by contrast, has a smaller SNR population (Filipović et al. 2008; Maggi et al. 2019; Titus et al. 2019; Joseph et al. 2019), and in particular, no obvious young (< 1000 yrs) type Ia SNRs (Roper et al. 2015; Sano et al. 2019b). The nearby Andromeda group (including M 31 and M 33) is too distant to allow the study of SN degeneracy scenarios (Galvin et al. 2012; Galvin and Filipovic 2014; Sasaki et al. 2018). As a result, LMC SNRs have been the subject of our considerable observational effort (Bojičić et al. 2007; Cajko et al. 2009; Crawford et al. 2008, 2010, 2014; Bozzetto et al. 2010; Grondin et al. 2012; Bozzetto et al. 2012b,c,a,d; de Horta et al. 2012; Haberl et al. 2012; Kavanagh et al. 2013; Bozzetto et al. 2013; De Horta et al. 2014a; Brantseg et al. 2014; Bozzetto et al. 2014a,b; Bozzetto and Filipović 2014; Warth et al.

2014; Maggi et al. 2014; Reid et al. 2015; Kavanagh et al. 2015c,b,a; Bozzetto et al. 2015; Kavanagh et al. 2016, 2019; Alsaberi et al. 2019; Maitra et al. 2019).

In this paper, we focus on N 103B, a young (380–860 yrs) SNR in the LMC (Rest et al. 2005). It is located close to a dense H II region (Chu and Kennicutt 1988), and only ~ 40 pc from the young star cluster NGC 1850 (Li et al. 2017). X-ray (Hughes et al. 1995), CO (Sano et al. 2018) and optical studies (Rest et al. 2005, 2008) have shown that it is likely to be a type Ia SNR; Li et al. (2017) observed a main sequence star that is likely to be the surviving companion. As shown in Figure 1, N 103B is not a simple spherical shell, showing significant structural asymmetries. The remnant has a diameter of 6.8 pc (Bozzetto et al. 2017), with the Western hemisphere that is ~ 3 times brighter than the Eastern hemisphere (Dickel and Milne 1995). The shell is Balmer-dominated in the optical wavelengths, which indicates the effects of propagating to a partially neutral circumstellar medium (CSM Ghavamian et al. 2017). N 103B is somewhat similar to the Kepler SNR, another young type Ia SNR (Reynolds et al. 2007). Recent morphological studies of H I and CO reinforce this picture, and suggest that the SN explosion occurred inside a medium heavily influenced by nearby OB stars and by the SN progenitor itself before it enters the WD stage (Sano et al. 2018).

Our paper is organised as following: Section 2 introduces our observations and data reduction. Section 3 shows our polarisation images of N 103B, discussing its implications for the supernova and its aftermath. In Section 4 we compare N 103B to similar young type Ia SNRs and finally conclusions are summarized in Section 5.

2 New ATCA Observations and augmented Data

The new and archival¹ ATCA observations of N 103B are now discussed. The data from two ATCA observation campaigns: one prior to the Compact Array Broadband Backend (CABB) upgrade (project C148), and the other using CABB (projects CX310, CX403, and C3229). Details of these observations are listed in Table 1.

C148 data (pre-CABB) include observations at 4786 and 8640 MHz over four days in 1992–1993, with four different arrays – 6A, 6C, 1.5D, and 1.5B respectively. Primary calibration (bandpass and flux density) used source PK B1934–638 for all four days, while

secondary calibration (phase) used source PKS B0407–658 for one day 27th Jun 1992, and PKS 0407–810 for the other three days. More details can be found in Dickel and Milne (1995). CABB data observations were made over three days in 2015–18, with different array configuration (6A, 6C, and EW352) at frequencies of 5500 and 9000 MHz. Primary calibration used source PKS 1934–638 (2015 and 2018) and PKS B0823–500 (2017). Source PKS B0530–727 was used as a secondary calibration for all CABB data. We reduced the data with the MIRIAD² (Sault et al. 1995) and KARMA³ (Gooch 1997) software packages.

We used the MIRIAD task *invert* with input parameter, *robust*, which has a range between −2 and 2, where: −2 is uniform weight, and 2 is natural weight. Robust has been selected to be 0 at 5500, 4786 and 9000 MHz; and 1 at 8640 MHz. MIRIAD tasks: *mfclean* and *restor* were used to clean and deconvolve CABB data, while the tasks *clean* and *restor* were used to clean and deconvolve pre-CABB data.

The resulting image properties from this reduction process are summarised in Table 2. The image at 4786 MHz is a combination of all four observing days, while at 8640 MHz we used only three days because of the strong radio-interference on 27th Jun 1992. This negatively affected the spatial resolution of this image. The images at 5500 and 9000 MHz combine three days of observations and have the lowest RMS noise due to favourable atmospheric conditions.

3 Results and Discussion

3.1 Radio morphology

Figure 2 (*left*) shows the ATCA (pre-CABB) image of SNR N 103B at 4786 MHz, overlaid with contours of 8640 MHz emission. The *right* panel shows the ATCA (CABB) image of SNR N 103B at 5500 MHz, with contours of 4786 MHz emission.

With a geometric centre of RA(J2000)=05^h08^m59.4^s and Dec(J2000)=−68°43'35", SNR N 103B shows a somewhat circular shell with significant morphological asymmetries. In particular, there are two bright regions toward the north-west and south-west. As we will discuss further in Section 4, N 103B is morphologically distinct to other young (~ 400 yrs; Roper et al. 2018) type Ia SNR, which are generally much more symmetric.

²<http://www.atnf.csiro.au/computing/software/miriad/>

³<http://www.atnf.csiro.au/computing/software/karma/>

¹Australia Telescope Online Archive (ATOA), hosted by the Australia Telescope National Facility (ATNF): atnf.atnf.csiro.au

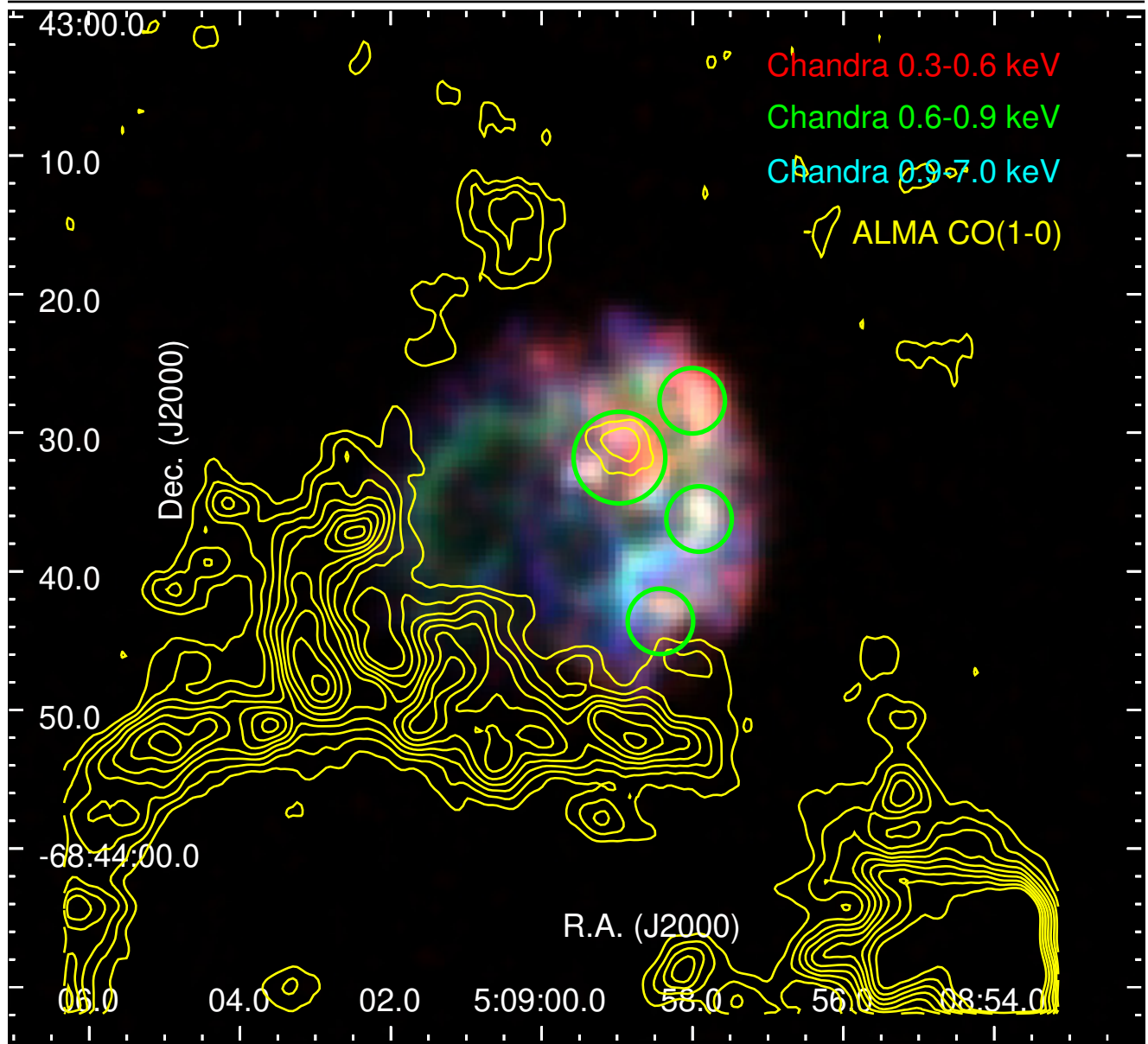


Fig. 1 Three-colour image of Chandra X-ray emission from N 103B (Lewis et al. 2003). The colours represent three energy bands: 0.3–0.6 keV, 0.6–0.9 keV, and 0.9–7.0 keV (red, green, and blue, respectively). Yellow contours correspond to ALMA CO(1–0) emission integrated between 244.8 and 252.8 km s^{-1} (contour levels are $5, 10, \dots, 45 \text{ K km s}^{-1}$), and indicate the potential molecular gas association found by Sano et al. (2018). Four circles show regions containing optical nebula knots, as seen in the HST H α emission (Li et al. 2017).

3.2 Radio spectral index

SNR radio spectra can often be described as a pure power-law of frequency: $S_\nu \propto \nu^\alpha$, where S_ν is flux density, ν is frequency, and α is the spectral index. Such a simple mathematical form stems from the test-particle diffusive shock acceleration (DSA) theory (Axford et al. 1977; Krymskii 1977; Bell 1978; Blandford and Ostriker 1978). To more accurately measure the spectral index of our source, we combine our observations with flux density measurements across a wide range of frequen-

cies from the Murchison Widefield Array (MWA; For et al. 2018); 84–200 MHz and Molonglo, Parkes and ATCA (408–14700 MHz), as shown in Table 3.

In Figure 3 (*left*) we plot N 103B flux density vs. frequency. The relative errors (assumed 10% uncertainty in all flux density measurement) are used for the error bars on a logarithmic plot. The best power-law weighted least-squares fit is shown (thick black line), with the spatially integrated spectral index $\langle \alpha \rangle = -0.75 \pm 0.01$ which is marginally higher, but still con-

Table 1 ATCA observational data of SNR N 103B.

Date	Project Code	Array Configuration	No. Channels	Bandwidth (GHz)	Frequency ν (MHz)	References
1992 Jun 27	C148	6A	33	0.128	4786	Dickel and Milne (1995)
1993 Feb 21	C148	6C	33	0.128	4786, 8640	Dickel and Milne (1995)
1993 Mar 15	C148	1.5D	33	0.128	4786, 8640	Dickel and Milne (1995)
1993 Mar 20	C148	1.5B	33	0.128	4786, 8640	Dickel and Milne (1995)
2015 Jan 01	CX310	6A	2049	2.048	5500, 9000	Our observation
2017 Dec 25	CX403	6C	2049	2.048	5500, 9000	Our observation
2018 Mar 27	C3229	EW352	2049	2.048	5500, 9000	Our observation

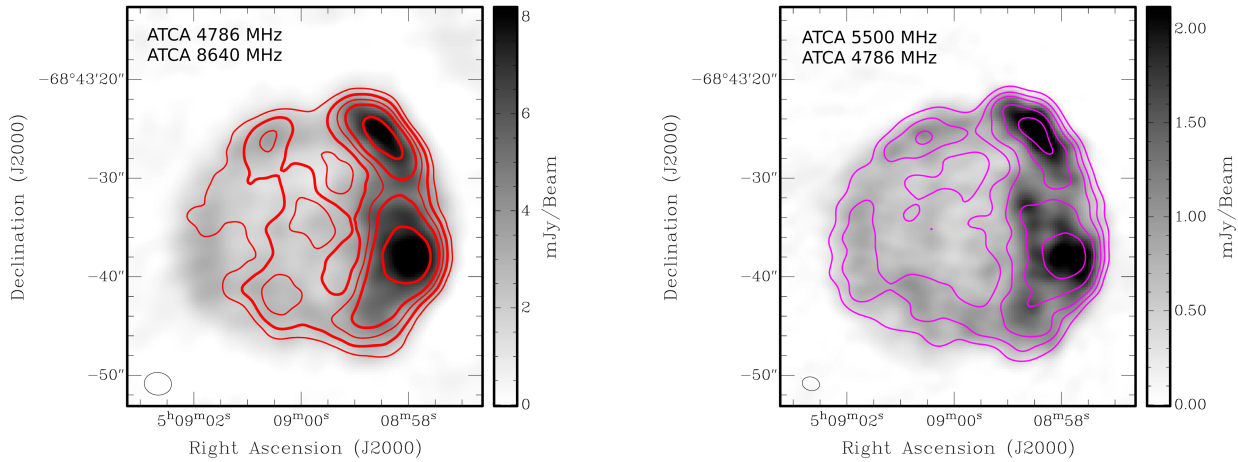


Fig. 2 ATCA (pre-CABB) image of SNR N 103B at 4786 MHz (left) and CABB at 5500 MHz (right) overlaid with contour map at 8640 MHz (left; red) and 4786 MHz (right; magenta). The red contour levels are: 1.5, 2, 2.5, 3, and 4 mJy beam $^{-1}$ while the magenta contour levels are: 1.5, 2.5, 3.5, 5.5, and 7.5 mJy beam $^{-1}$. The ellipse in the lowest left corner is the synthesised beam of $2.^{\prime\prime}7 \times 2.^{\prime\prime}3$ and $1.^{\prime\prime}8 \times 1.^{\prime\prime}3$, respectively. The sidebar on the right hand side of each image represents the used gray scale gradient in mJy beam $^{-1}$. The RMS noise of the 4786 MHz image is 0.24 mJy beam $^{-1}$, 5500 MHz image is 0.031 mJy beam $^{-1}$, and 0.35 mJy beam $^{-1}$ in the 8640 MHz image.

sistent with the previous measured value of -0.67 of Dickel and Milne (1995). This steeper radio spectral index value is typical of young SNRs (Urošević 2014; Bozzetto et al. 2017). Actually, a couple of theoretical models have been proposed recently to account for such steep spectra observed in a significant number of young SNRs. These include oblique-shock effects (Bell et al. 2011), as well as the loss of cosmic-ray energy to turbulence and magnetic field at the non-relativistic quasi-parallel shocks (Bell et al. 2019). In addition, Pavlović (2017) demonstrated that the steep overall radio spectral index of SNR G1.9+0.3 can be explained only by means of the efficient non-linear diffusive shock acceleration (NLDSA).

Despite the actual scatter in data one can also discuss the apparent curvature in the overall radio spectrum. The curved radio spectra of young SNRs are usually interpreted as a result of an underlying NLDSA

process (Reynolds and Ellison 1992; Jones et al. 2003; De Looze et al. 2017). To model NLDSA effects on the global radio continuum spectrum, we used a simple varying power-law of the form $S_{\nu} \propto \nu^{\alpha+c \log \nu}$, where c represent a curvature parameter. The obvious better fit is obtained (see green dotted line in Figure 3 for NLDSA fit). It has a large curvature ($c = 0.16 \pm 0.03$) in comparison with the value of 0.03, for the case of Cas A (Onić and Urošević 2015). It is interesting to note that spatial variations in the spectral index in the case of Cas A remnant have also been proposed to be due to power-laws of different slopes rather than a single curved spectrum (Wright et al. 1999). In that sense, we also tried to interpret the integrated radio continuum of this remnant by assuming synchrotron radiation by two different cosmic-ray electron populations (TWO POP) that possibly reside in the SNR. In fact, we used a simple sum of two power-laws of the form

Table 2 Details of N 103B images used in this study

λ (cm)	ν (MHz)	Beam Size (arcsec)	RMS (mJy beam $^{-1}$)
6	4786	2.7×2.3	0.237
6	5500	1.8×1.3	0.031
3	8640	3.6×2.4	0.351
3	9000	1.10×0.85	0.022

Table 3 Flux density measurements of SNR N 103B at multiple frequencies

ν (MHz)	Flux Density S_ν (Jy)	Telescope	Reference
84	8.02	MWA	For et al. (2018)
107	4.95	MWA	For et al. (2018)
115	4.44	MWA	For et al. (2018)
118	4.69	MWA	For et al. (2018)
122	4.32	MWA	For et al. (2018)
130	4.19	MWA	For et al. (2018)
143	3.43	MWA	For et al. (2018)
150	3.45	MWA	For et al. (2018)
155	3.42	MWA	For et al. (2018)
158	3.11	MWA	For et al. (2018)
166	2.94	MWA	For et al. (2018)
173	3.10	MWA	For et al. (2018)
189	2.59	MWA	For et al. (2018)
196	2.65	MWA	For et al. (2018)
200	2.80	MWA	For et al. (2018)
408	1.57	Molonglo	Bozzetto et al. (2017)
843	0.613	MOST	Bozzetto et al. (2017)
1377	0.496	ATCA	Bozzetto et al. (2017)
4750	0.429	Parkes	Bozzetto et al. (2017)
4800	0.217	ATCA	Bozzetto et al. (2017)
4850	0.426	Parkes	Bozzetto et al. (2017)
5000	0.360	Parkes	Bozzetto et al. (2017)
5500	0.380	ATCA	This work
8550	0.226	Parkes	Bozzetto et al. (2017)
8640	0.138	ATCA	Bozzetto et al. (2017)
9000	0.130	ATCA	This work
14700	0.16	Parkes	Bozzetto et al. (2017)

$S_\nu = S_1\nu^{\alpha_1} + S_2\nu^{\alpha_2}$. The fit is even better in this case but requires a very high value for a steeper spectral index ($\alpha_1 = -1.90 \pm 0.40$, $\alpha_2 = -0.58 \pm 0.07$), that is not usually seen in SNRs (see red dashed line in Figure 3 for TWO POP. fit). Of course, a high scatter in data points especially between 4–5 GHz prevent us from making firm conclusions on the particle acceleration properties based solely on the integrated radio continuum. For all the weighted least-squares fitting of the radio continuum we have used the MPFIT⁴ (Markwardt 2009) package written in IDL, with starting values estimated from the data.

On the other hand, the analysis of spatial variations in the radio continuum spectral index within the SNR is very important (see e.g. discussion on the properties of SNRs Tycho, Cas A, as well as SN 1978A; Katz-Stone et al. 2000; Anderson and Rudnick 1996; Zanardo et al. 2013). Such spatial variations are generally linked to the electron acceleration processes that among other processes depend on the evolution of the SNR. It can be concluded that the synchrotron radio spectral index traces the distribution of energy among cosmic-ray electron populations and can probe the compression ratio of the shock on a local scale. That is why we can use these results to study properties of the particle acceleration mechanisms. In that sense, understanding of the spatial variation of the spectral index and emission across young SNRs is imperative.

Figure 3 (*right*) shows a map of the spectral index for N 103B. It can be seen that the spectral index distribution across the remnant is not at all uniform. The spectral index is shallower (between -0.7 and -0.8) in the bright regions on the Western side of N 103B, and steeper in the centre and Eastern side of the SNR (from -0.8 to around -0.9 ; $0.1 < \Delta_\alpha < 0.2$). This could indicate different emission and/or particle acceleration scenarios for different regions (various population of electrons are contributing). It should be noted that the steep spectral indices are also observed in the regions where SNR interact with molecular environment as seen in Figure 1, contrary to the usual expectations that involve simple compression (amplification) of magnetic field. This is somewhat similar to what we observed in the case of Galactic SNR Vela Jr. (Maxted et al. 2018) and LMC SNR N 63A (Sano et al. 2019a). However, both of these SNRs are most likely result of CC explosion. If the electron energy spectrum hardens at lower frequencies, regions in which the magnetic field is higher than the surroundings will both appear brighter and have a flatter spectrum than the surroundings. Actually, regions in which the magnetic field is stronger

⁴<http://purl.com/net/mpfit>

would appear both brighter and with a flatter spectrum. Of course, if the shock wave is significantly decelerated due to the interaction with the molecular cloud environment, we expect less efficient particle acceleration which leads to the steeper radio spectral indices. In addition, optical images show H α emission along the entire periphery of the Western portion of the shock, with [O III] and [S II] lines emitted from a few dense clumps where the shock has probably become radiative (Williams et al. 2014). These regions coincide with spectral indices between -0.7 and -0.8.

An important clue for this analysis can be found in the linear polarisation maps at 5500 and 9000 MHz discussed in Section 3.4 (see also Figure 4). Linear polarisation is detected mainly where the emission is brightest, in the Western part of the remnant. However, a bit less pronounced linear polarisation is also seen in the Eastern parts of the SNR. Radial and oblique orientation of the ordered magnetic field is more dominant in the regions of high radio and X-ray emission (Western parts). Quasi-perpendicular shock geometries are more pronounced in the Eastern parts of the SNR, which can explain less efficient particle acceleration in these regions. Still, we note that Caprioli et al. (2018) have showed that the high-energy particles can be effectively reflected and accelerated regardless of shock inclination via so-called diffusive shock re-acceleration process. They found that re-accelerated Galactic cosmic rays can drive the streaming instability in the shock upstream and produce effective magnetic field amplification. This can then trigger the injection of thermal particles even at quasi-perpendicular shocks.

Finally, a word of caution regarding this discussion. As the estimated uncertainty for the measured spectral indices is between 0.1–0.2, it is therefore not possible to draw any firm conclusions about this issue. Especially, we note that the steepest α regions are correlated with the lowest signal to noise regions.

3.3 Expansion

There are many difficulties measuring the expansion rate for the SNR shell, because the CABB and pre-CABB data were taken using different instrument setups and different band-passes. Therefore, differences in SNR shell size at different epochs (about 26 years apart) are difficult to disentangle from the above mentioned observational and instrumental effects.

Nevertheless, we can place limits on the expansion velocity of the shell. We compare the pre-CABB data with the CABB image data, smoothing the lower spatial resolution pre CABB image data (4786 MHz) to the higher resolution of the CABB data (5500 MHz)

for an equivalent full width half maximum (FWHM) of 0.5–1 arcsec resolution. If we interpret the resulting differences in our radio images as due to motion (rather than due to brightening, intrinsic or instrumental), then our estimate of the expansion velocity is in range of 4000–9000 km s $^{-1}$, this value is consistent with the result of Williams et al. (2018) 4170 $^{+1280}_{-1310}$ km s $^{-1}$ (~0.017 arcsec yr $^{-1}$), which are based on Chandra X-ray observations.

3.4 Polarisation

Polarisation is calculated using the Stokes parameters:

$$P = \frac{\sqrt{S_Q^2 + S_U^2}}{S_I}, \quad (1)$$

where P is the mean fractional polarisation, S_Q , S_U , and S_I are integrated intensities for the Q , U , and I Stokes parameters. The overall fractional polarisation of N103B is 8±1% at 5500 MHz and 13±3% at 9000 MHz. This is somewhat higher than the value of 5% determined by Dickel and Milne (1995) at 4786 MHz. However, we emphasise that the ATCA polarisation capabilities back in 1992–1993 were significantly lower. Also, the depolarisation effect might play a role caused by differential Faraday rotation.

Figure 4 shows polarisation intensity map at 5500 MHz (4a), fractional polarisation map at 5500 MHz (4b), polarisation intensity map at 9000 MHz (4c), and fractional polarisation map at 9000 MHz (4d). All polarisation images haven't been corrected for Faraday rotation. The average polarisation intensity at 5500 and 9000 MHz are ~0.09 and ~0.05, respectively. The fractional polarisation map at 5500 MHz reveals linear polarisation, particularly where the emission is brightest in the east and north-west of the remnant. This probably indicates the existence of coherent magnetic fields where the shell impacts the ISM. The 9000 MHz images show lower levels of polarisation, but a similar pattern of intensity and direction with respect to the radio emission.

Note an exception: the bright structure towards the west (marked with red ellipse) is (total intensity) bright but unpolarised. This structure is obvious in our new CABB images but unclear in pre-CABB images. This is due to the fact that our new CABB images have better resolution and lower RMS noise. Another possibility, however less likely, is that this region either brightened or expanded significantly faster than the rest of this remnant. The lack of polarisation may indicate intense radio thermal emission coming from this region.

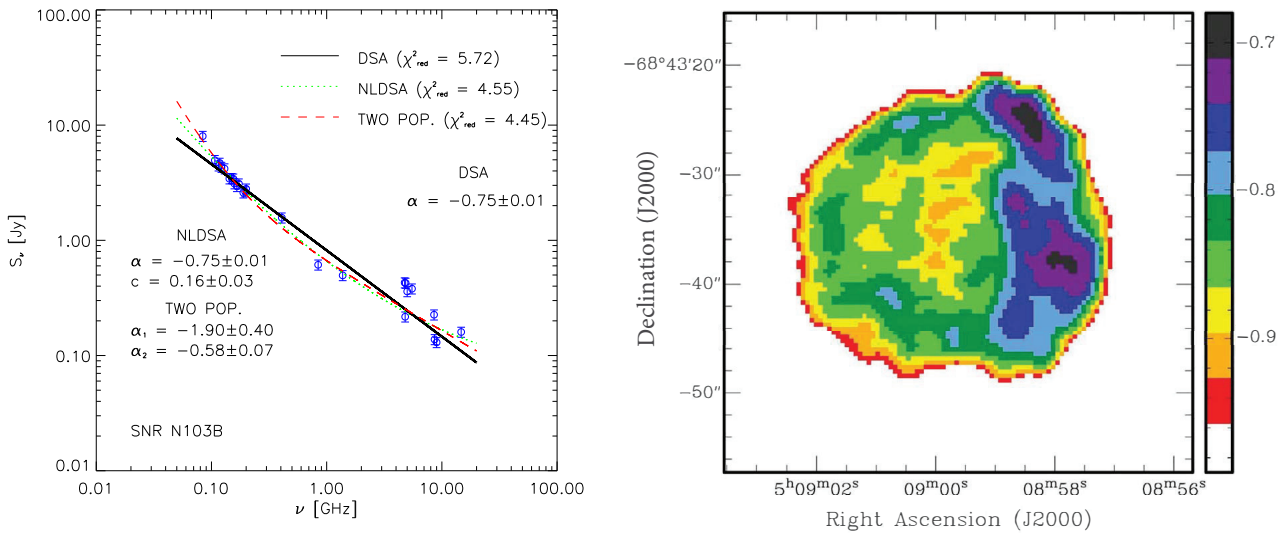


Fig. 3 *Left:* Radio continuum spectrum of SNR N103B, from MWA and ATCA data (Table 3). The black solid line shows a linear least squares fit in logarithmic space, giving the spatially integrated spectral index of $\langle \alpha \rangle = -0.75 \pm 0.01$. The simple NLDSA model is represented by a green dotted line, while the model that assumes two different populations of electron is shown as a dashed red line. The relative errors (assumed 10% uncertainty in each flux density measurement) are used for the error bars on a logarithmic plot. *Right:* Spectral index map for N103B at 5500 MHz, showing a shallower index where the emission is brightest. The uncertainty in α is < 0.2 .

3.5 Faraday Rotation and Magnetic Field

We can measure interstellar magnetic fields through their effect on the propagation of linearly polarized radiation. As the polarized emission from a radio source passes through a magnetized, ionized plasma, the plane of polarization rotated due to the different phase velocities of the two polarization modes. This Faraday rotation changes the position angle of the emission by an amount which depends on the rotation measure (RM):

$$RM = 811.9 \int_0^L n_e B_{\parallel} dl , \quad (2)$$

where RM is in rad m^{-2} , n_e is the electron density in cm^{-3} , B_{\parallel} is the line of sight magnetic field strength in μG , and L is the path length through the Faraday rotating medium in kpc. The change in position angle of the radiation is:

$$\Delta_X = X - X_0 = RM \lambda^2 , \quad (3)$$

Where X is the observed position angle at wavelength λ , and X_0 is the intrinsic position angle of the polarized emission. To overcome the $n \pi$ ambiguity in measurements of the position angle, we require observations at three or more wavelengths (Clarke 2004). To calculate RM, we split the 2048 MHz bandwidth at 5500 MHz into three 680 MHz sub bands (4817, 5500, and 6183 MHz).

Figure 5 shows the measured RM for N103B. The mean value for RM in this SNR is $200 \pm 20 \text{ rad m}^{-2}$ (with a peak of $\approx 460 \text{ rad m}^{-2}$). Similar to the polarisation, the greatest rotation measure can be seen close to where the total intensity emission is brightest.

Having measured RM, we can use Equation 2 to estimate the magnetic field strength. Table 4 summarizes different estimates of the electron density of N103B. Li et al. (2017) estimated the mean electron number density toward the optical knots or post-shock gas of N103B to be $\sim 500\text{--}5000 \text{ cm}^{-3}$. Williams et al. (2014) calculated the post-shock gas's electron number density to be $\sim 45 \text{ cm}^{-3}$ using IR data. Someya et al. (2014) estimated the plasma electron number density to be $\sim 10\text{--}47 \text{ cm}^{-3}$, while the estimate by van der Heyden et al. (2002) is $\sim 7\text{--}25 \text{ cm}^{-3}$ and Someya et al. (2014) reported an electron number density of $\sim 2\text{--}10 \text{ cm}^{-3}$ in the ambient gas (pre-shock density). Therefore, the Faraday rotation is through the shocked ionised gas, and thus the n_e relevant is 4 times that value. That would make it $\sim 8\text{--}40 \text{ cm}^3$, so closer to van der Heyden et al. (2002) or Williams et al. (2014) estimate, and narrow down the range of magnetic field. There is no doubt that the range of n_e shows wide varieties but some are less applicable than others. The one for the optical knots (high n_e) are for small clumps and not likely representing the overall medium density.

Using the average value of RM (200 rad m^{-2}), and L as the thickness of the compressed shell of the SNR

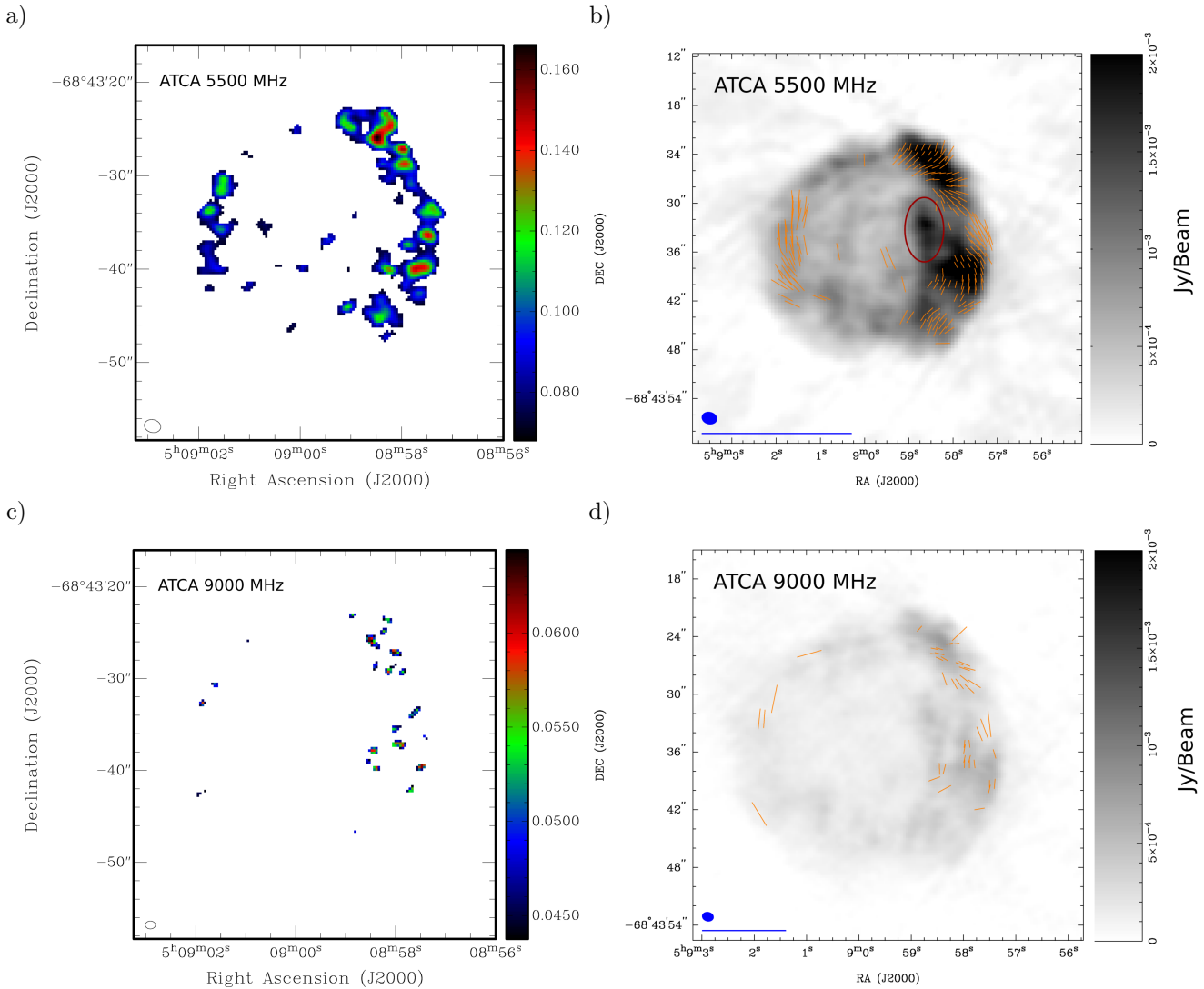


Fig. 4 a) Polarisation intensity map of SNR N 103B at 5500 MHz. The ellipse in the lower left corner shows the synthesised beam of $1.^{\circ}8 \times 1.^{\circ}3$. b) Fractional Polarisation vectors (orange) overlaid on top of the intensity map (gray scale) of SNR N 103B at 5500 MHz. The blue ellipse is similar to (a) and the blue line below the ellipse represents 100% polarisation. Interestingly, we note a radio thermal emission toward the west (red ellipse). c) Polarisation intensity map of SNR N 103B at 9000 MHz. The ellipse in the lower left corner shows the synthesised beam of $1.^{\circ}1 \times 0.^{\circ}85$. d) Fractional Polarisation vectors (orange) overlaid on top of the intensity map (gray scale) of SNR N 103B at 9000 MHz. The blue ellipse is similar to (c) and the blue line below the ellipse represents 100% polarisation.

(~ 1.5 pc), we find that the magnetic field strength values for N 103B vary from $0.03 \mu\text{G}$ to $82.1 \mu\text{G}$, with most values clustered around $16.4 \mu\text{G}$. The specific values are shown in Table 4.

We also use the equipartition formulae⁵ (Arbutina et al. 2012; Arbutina et al. 2013; Urošević et al. 2018) to estimate the magnetic field strength for this SNR. This derivation is purely analytical, accommodated especially for the estimation of the magnetic field strength in SNRs. The average equipartition field over the whole

shell of N 103B is $\sim 235 \mu\text{G}$ with an estimated minimum energy⁶ of $E_{\min}=6.3 \times 10^{48}$ erg. This value is typical of young SNRs with a strongly amplified magnetic field. For example, its cousin and neighbouring LMC SNR J0509–6731 has an estimated average equipartition magnetic field strength of $\sim 168 \mu\text{G}$ (Bozzetto

⁵<http://poincare.matf.bg.ac.rs/~arbo/eqp/>

⁶We use the following N 103B values: $\theta=0.24'$, $\kappa = 0$, $S_{1 \text{ GHz}}=0.903$ and $f=0.25$; for $\kappa \neq 0$ we estimate the average equipartition field of $396 \mu\text{G}$ with an estimated minimum energy of $E_{\min}=1.8 \times 10^{49}$ erg which is probable overestimate, because physical background gives better equipartition arguments for $\kappa = 0$ (Urošević et al. 2018).

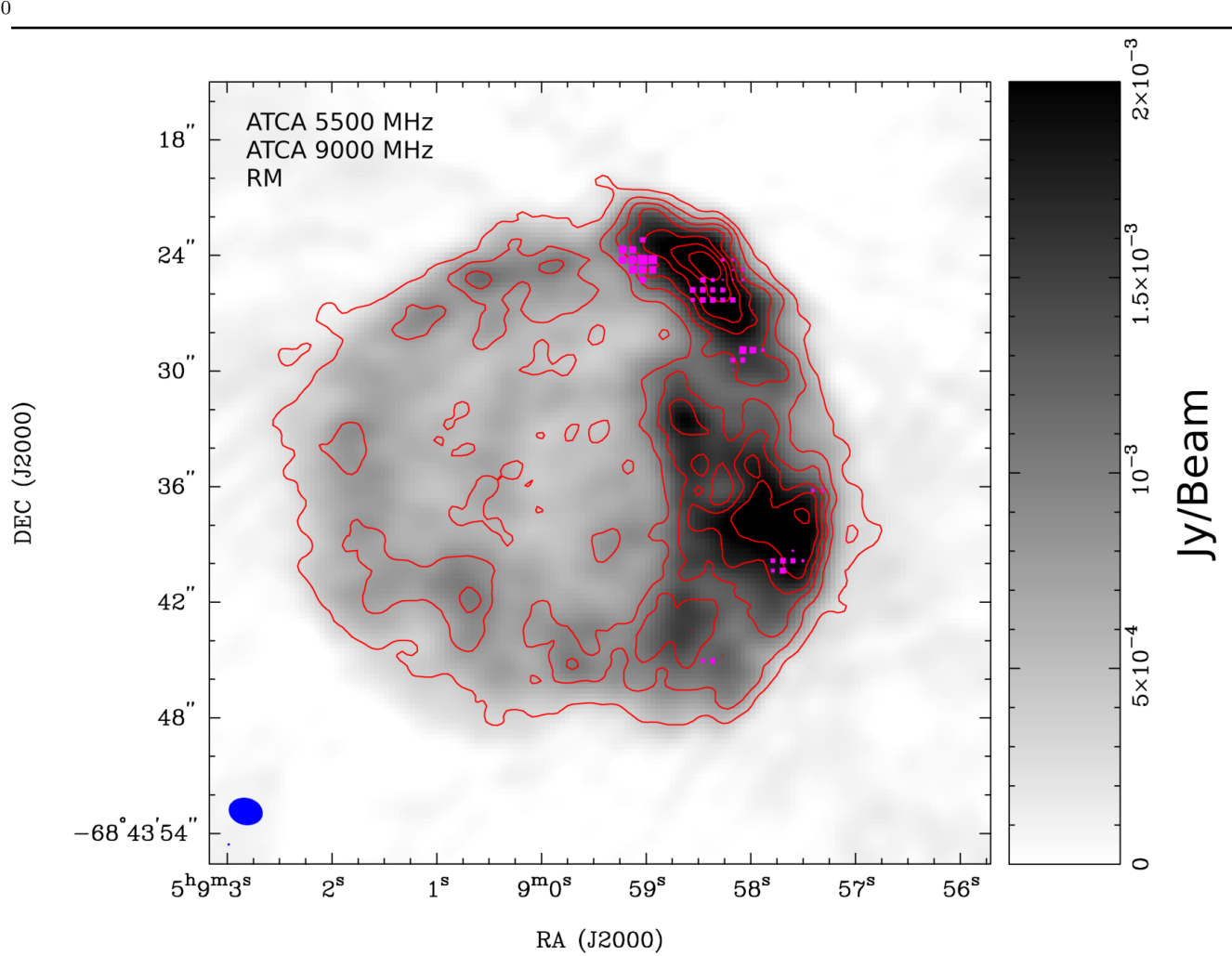


Fig. 5 SNR N103B at 5500 MHz (gray scale) overlaid with 9000 MHz contours. The contour levels are: 0.1, 0.2, 0.3, 0.4, 0.5, 0.6 and 0.7 mJy beam $^{-1}$. The pink boxes represent RM estimated from position angles associated with linear polarisation. All boxes have positive values, the maximum value of RM is ≈ 460 rad m $^{-2}$. The blue ellipse in the lower left corner represents the synthesised beam of $1.^{\prime\prime}8 \times 1.^{\prime\prime}3$

et al. 2014b), while the much older (20–25 kyr) type Ia MCSNR J0508–6902 has a magnetic field strength of ~ 28 μ G (Bozzetto et al. 2014a) or the middle-aged MC-SNR J0530–7007 where de Horta et al. (2012) estimated the equipartition magnetic field over the whole shell to be ~ 53 μ G.

3.6 H α and X-ray Emission

In Figure 6 we compare our new ATCA 5500 MHz radio continuum observations to Hubble Space Telescope H α emission (Li et al. 2017), and Chandra ‘soft’, ‘medium’ and ‘hard’ X-ray emission (0.3–0.6, 0.6–0.9 and 0.9–7.0 keV, respectively). Li et al. (2017) have previously shown thermal emission in H α that corresponds to soft X-ray emission seen by Lewis et al. (2003), and is particularly prominent towards regions with dense optical

Table 4 Electron density and magnetic field strength for N103B based on various estimates for the electron density

n_e (cm $^{-3}$)	References	B (μ G)
500–5000	Li et al. (2017)	0.3–0.03
45	Williams et al. (2014)	3.6
10–47	Someya et al. (2014)	16.4–3.4
7–25	van der Heyden et al. (2002)	23.5–6.6
2–10	Someya et al. (2014)	82.1–16.4

knots. These thermal signatures of an ionised circumstellar medium are not expected to correspond to the N 103B radio emission which traces a non-thermal component from electrons accelerated by the SNR shock.

Nevertheless, some correlation between radio continuum and hard non-thermal X-rays is expected. As seen in Figure 6d (0.9–7.0 keV), the hard X-ray emission follows the radio emission, but not particularly closely. Although the large-scale structure of N 103B radio continuum emission is evidently enhanced in the Western part of SNR, comparing with other two frequency (optical and X-ray) emissions no exact/precise matching can be seen. There are many lines (Ne, Mg, Si, S, Ar, even Fe K) in 0.9–7.0 keV band, which actually most likely dominates the emission from N 103B. Perhaps, this is the main reason why even in that band they are no particularly striking radio-to-X-ray match.

4 Comparison to Similar Age and Type Ia SNRs

We compare the morphological and physical characteristics of young type Ia SNRs including their symmetry, average fractional polarisation, alignment between X-ray, optical & radio emission distribution to degeneracy models as listed in Table 5. Although, no firm evidences for surviving progenitor companions have been found in any of the proposed young type Ia SNRs, we ‘predict’ the most likely degeneracy scenarios based on common characteristics as found in the literature and respective assumptions therein⁷. Table 5 shows young (age ≤ 1000 years) type Ia SNRs in the Milky Way and the LMC.

Diameter: The SNRs from our sample show reasonably similar sizes, which most likely reflects our selection criteria of being young age (≤ 1000 yrs). Using the usual linear (or slightly less than linear) expansion and assuming a canonical SN energy of 10^{51} ergs, the spread in diameter could be more reflecting different ages and explosion energy.

Spectral Index: The spectral index (α) is similar for the SNRs, with a slight preference for older SNR having shallower spectral indices. In particular, N 103B is very similar to J0509–6731, with $\alpha = -0.73 \pm 0.02$ (Bozzetto et al. 2014b).

Similarly, the radio spectral index among young type Ia SNRs (see Table 5) varies from -0.81 in the

youngest Galactic SNR G1.9+0.3 to -0.6 in the oldest (SN1006). As expected, the steepness of the radio spectral index is proportional to their still young age, but we don’t see any obvious connection between the proposed degeneracy model and spectral index.

Morphology: The Galactic environment plays an important role in the morphological characteristics of an evolving SNR. Intriguingly, the six other young type Ia SNRs from this sample are significantly more circular and symmetric than N 103B. Lopez et al. (2011) suggested a link between the spherical thermal X-ray morphology and the remnant type, where those SNRs resulting from a type Ia SN explosion were more spherical than those from CC supernovae. However, we shouldn’t forget that at such young age of their evolution (< 1000 yrs) any SNR would keep its circular shape to some degree (Bozzetto et al. 2017).

J0509–6731, exhibits an almost circular (‘doughnut’) morphology of 7.4 pc, with brightened regions towards the south-western limb and a second brightened inner ring which is only seen in the radio continuum (Bozzetto et al. 2014b; Roper et al. 2018). We see a very similar morphology in all other young type Ia SNRs from our sample except N 103B, which shows an obvious asymmetric distribution as described earlier.

We note that J0509–6731 and N 103B, are positioned $\sim 1.5^\circ$ and $\sim 0.5^\circ$ respectively from the LMC’s main optical bar. We might expect the expansion rate of N 103B to be less than that of J0509–6731, since it is located closer to the mid-plane of the LMC where the density of cold gas and dust is typically higher than in the outer regions of dwarf irregular galaxies. This cold gas may be the result of in-fall but due to secular evolutionary processes eventually compressed to form stars and at time-scales (\sim Gyr) due to Galactic disk instabilities form bar and spiral structure typically found in many disk galaxies. This in turn could also explain the fact that the outer radio emission of N 103B is asymmetric and the lower fractional polarisation found around N 103B as compared to J0509–6731 since wind speeds would become truncated.

The angular size of type Ia SNRs at this critical stage of evolution shows interesting tendencies. Apart from the oldest (SN1006) and youngest (G1.9+0.3) SNRs from our sample, all five other SNRs have the same size of 7–8 pc. Morphologically, we can see the evidence that N 103B as a type Ia SD explosion is unique (among this sample) for its asymmetric appearance. A plausible explanation, assuming the SN explosion is of the SD type, is that the nearby giant companion star may have preferentially ‘blocked’ the explosion front from freely propagating in one direction, while in the other having evolved relatively ‘unobstructed’ into the ISM. On

⁷We also emphasise that most of these young SNRs have no firm type Ia classification either.

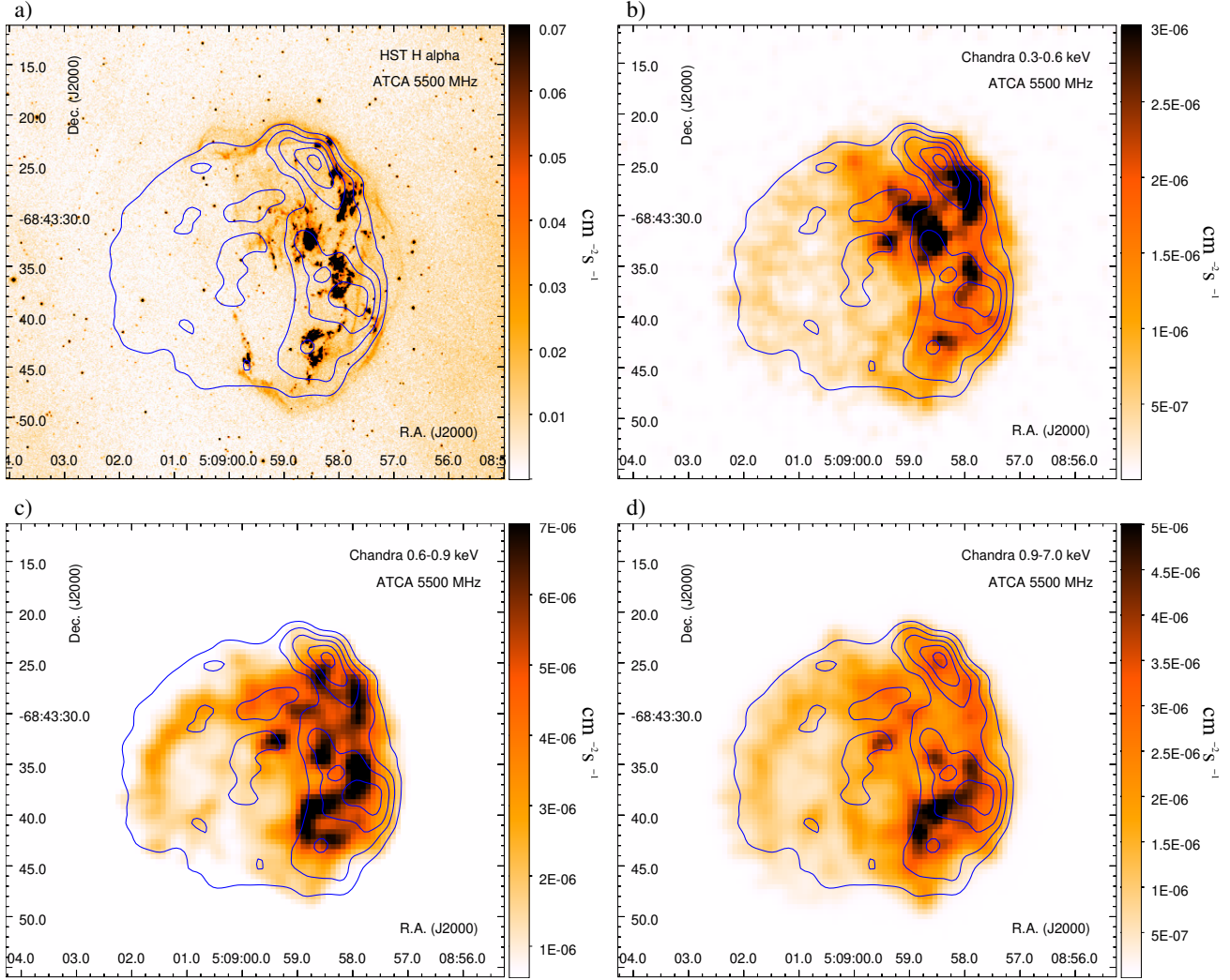


Fig. 6 a) Hubble Space Telescope H α image of N 103B (Li et al. 2017). b), c) and d) Chandra 0.3–0.6, 0.6–0.9 and 0.9–7.0 keV images of N 103B (Lewis et al. 2003). All images have ATCA 5500 MHz radio continuum contours (this study) overlaid.

average, this would make DD expansion velocities significantly larger than they would be for SD events with apparent radii somewhat larger for a fixed age. However, most hydro-dynamical simulations of SN type Ia shock propagating show that a gap from the presence of the companion is quickly ‘forgotten’. It’s more likely that the asymmetrical structure of N 103B comes from the larger scale environment (possibly affected by the progenitor system winds).

Polarisation and Magnetic Field: The expectation is that the type Ia SNR is expanding into a homogeneous regular magnetic field and it is evolved in such a way that the ambient medium dominates the expansion. The RM around the shell should be the same, with a gradient along the shell depending on the angle between the ambient magnetic field and the plane of the

sky. In the case of a very young SNR, the magnetic field should be radial in 3-D space, in which case RM symmetry should be observed. However, in our case the magnetic field is concentrated in the Western side of the remnant (figure 4). Therefore, we notice that the RM is distributed in the west-side of the remnant only (figure 5).

Bozzetto et al. (2014b) estimated the P value for J0509–6731 at 5500 MHz of $26 \pm 13\%$, which is somewhat higher than the value for N 103B ($\sim 8\%$ at 5500 MHz). This may be weakly correlated to age, since J0509–6731 is a younger SNR (almost half the age of N 103B). However, the same fractional polarisation value has been observed in another young LMC SNR – LHG 26 – both remnants are of approximately the same age (Table 5). On the other hand, the young Galactic

Table 5 Young (≤ 1000 yrs) type Ia SNRs in Galaxy (MW) and LMC. The proposed degeneracy scenario listed in Column 8 are abbreviated as SD for single degenerate and DD for double degenerate type Ia explosion. No firm evidence of surviving companions have been found in any of these SNRs. We note that different methods were used to estimate of the SNRs magnetic field.

SNR Name	Host Galaxy	Age (year)	Diameter (pc)	Distance (kpc)	Spectral Index (α)	Avg. Polarisation (%)	Mag. Field (μG)	Deg. Type
Tycho	MW	425 ¹	3.5–7.2 ¹	1.5–3.1 ¹	-0.58 ²	20–30 at 4872 MHz ³	50–400 ⁴	DD ⁵
SN1006	MW	1000 ⁶	$\sim 19^6$	$\sim 2.18^6$	-0.6 ²	~ 17 at 1400 MHz ⁷	30–40 ⁸	DD ⁹
Kepler	MW	407 ¹⁰	$\sim 8.18^{10}$	$\sim 7^{10}$	-0.64 ²	~ 6 at 4835 MHz ¹¹	$\sim 414^{12}$	SD ¹³
G1.9+0.3	MW	$\sim 120^{14}$	4 ¹⁵	8.5 ¹⁵	-0.81 ¹⁶	6 at 5500 MHz ¹⁷	273 ¹⁷	DD ¹⁸
J0509–6731	LMC	$\sim 310^{19}$	7.4 ²⁰	50	$\sim -0.73^{20}$	~ 26 at 5500 MHz ²⁰	168 ²⁰	DD ²¹
LHG 26	LMC	$\sim 600^{22}$	8.3 ²²	50	$\sim -0.54^{23}$	~ 8 at 5500 MHz ²³	$\sim 171^{23}$	DD ²⁴
N 103B	LMC	380–860 ²⁵	6.8 ²⁶	50	~ -0.75	~ 8 at 5500 MHz	0.03–82.1	SD ²⁷

References: (1) Hughes (2000), (2) Green (2014), (3) Dickel et al. (1991), (4) Tran et al. (2015), (5) Woods et al. (2017), (6) Winkler et al. (2003), (7) Reynoso et al. (2013), (8) Vink (2006), (9) Kerzendorf et al. (2018), (10) Patnaude et al. (2012), (11) DeLaney et al. (2002), (12) Arbutina et al. (2012), (13) Meng and Li (2019), (14) Pavlović (2017), (15) Reynolds et al. (2008) (16) Luken et al. (2019; in prep), (17) De Horta et al. (2014b) (18) Borkowski et al. (2013), (19) Roper et al. (2018), (20) Bozzetto et al. (2014b), (21) Schaefer and Pagnotta (2012), (22) Borkowski et al. (2006), (23) Bozzetto et al. (2012d), (24) Edwards et al. (2012), (25) Rest et al. (2005), (26) Bozzetto et al. (2017), and (27) Ghavamian et al. (2017).

SNRs show a disparity in P values. The P value for the youngest Galactic SNR (G1.9+0.3) is very low in comparison to Tycho and SN 1006 (see Table 5). While the diversity in P values might be due to the difference in the ambient density and age, it also may indicate different types of SNe. Specifically, Luken et al. (2019; in prep) show that the alleged type Ia SNR G1.9+0.3 might actually be the product of a core collapse SN based on RM, shape and strength of its polarisation vectors.

Previous estimates of magnetic field strength in N 103B vary between 0.03–82.1 μG (Table 4). Yet a stronger equipartition field of 168 μG was estimated for J0509–6731 by Bozzetto et al. (2014b), which is still lower than our estimate of N 103B $\sim 235 \mu\text{G}$. A similar situation can be seen in other type Ia SNRs (Table 5). Although this SNR is a relatively young one, the equipartition assumption is not so proper for the determination of the magnetic field strength (it can be estimated only to an order of magnitude (see Urošević et al. 2018)). In any case, the estimated value of 168 μG can be explained by the magnetic field amplification at the strong shock of the relatively young and highly luminous SNR. Based on the young type Ia SNRs in this study, we can not see any clear differences in polarisation nor magnetic field strength that would lead us to conclude a distinct difference between single or double degenerate SN scenarios. However, further studies with larger sample sizes and better constrained parameters are required to conclusively rule out any connection.

The surface brightness to diameter diagram: The position of LMC SNR N 103B in the surface brightness to diameter (Σ – D) diagram ($\Sigma=6\times 10^{-19} \text{ W m}^{-2} \text{ Hz}^{-1} \text{ sr}^{-1}$, $D=6.8 \text{ pc}$) by Pavlović et al. (2018), suggests that this

remnant is in the early Sedov phase, with an explosion energy of $1\text{--}1.5\times 10^{51} \text{ erg}$, which evolves in an environment with a density of $0.02\text{--}0.2 \text{ cm}^{-3}$. These values are as expected if N 103B is interacting with a molecular cloud (Sano et al. 2018) where the average density is somewhat higher compared to the rest of type Ia SNRs.

This result is also in a good accordance with the observed steep overall radio spectral index. Actually, particle acceleration is most efficient exactly in the early stage of the Sedov-Taylor phase. In fact, in this evolutionary stage, the particle acceleration is more efficient than in the ejecta dominated free expansion phase.

Our estimate of N 103B surface brightness (Σ) is comparable to values found for Galactic remnants in rarefied environments, such as LMC SNR J0509–6731 ($\Sigma=1.1\times 10^{-19} \text{ W m}^{-2} \text{ Hz}^{-1} \text{ sr}^{-1}$, $D=7.4 \text{ pc}$), Tycho's SNR ($\Sigma=1.32\times 10^{-19} \text{ W m}^{-2} \text{ Hz}^{-1} \text{ sr}^{-1}$, $D=7.4 \text{ pc}$) and Kepler's SNR ($\Sigma=3.18\times 10^{-19} \text{ W m}^{-2} \text{ Hz}^{-1} \text{ sr}^{-1}$, $D=8.18 \text{ pc}$; Pavlović et al. (2013)).

5 Conclusions

In this paper, we produced new radio continuum images for the young LMC SNR N 103B using ATCA CABB data and compared them with pre CABB images. Our new images are of higher resolution and more sensitive than previous images obtained by Dickel and Milne (1995).

We estimated N 103B radio spectral index of -0.75 ± 0.01 and found its shape to be concave-up. We suggest that the most likely reason is the NLDSA effects or presence of two different population of ultra-relativistic electrons.

We found that the radio morphology for this SNR is asymmetric which is different from other young type Ia

LMC SNRs such as J0509–6731 or LHG 26, which exhibit a circular morphology.

We place an upper limit on the expansion velocity of the SNR shell and found our value to be consistent with that determined for higher spatial resolution using X-ray data. We detect that the SNR N 103B shows localized linear polarisation, especially in the north-west side of the remnant. The average fractional polarisation for N 103B at 5500 MHz is $8\pm1\%$, which is slightly higher than the value found by Dickel and Milne (1995) due to higher sensitivity. We also estimate the P value at 9000 MHz to be $13\pm3\%$. Interestingly, we found unpolarised clumps towards the south-west bright region (Figure 4) which might be a relic of the initial explosion. Our new α value for N 103B is consistent with that of previous studies of -0.75 ± 0.01 and inline with other young type Ia SNRs.

In order to estimate the strength of the magnetic field for this SNR, we calculated RM at three frequencies (4817, 5500, and 6183 MHz). The mean value of RM was $200\pm20 \text{ rad m}^{-2}$ and we estimated the magnetic field strength for this SNR to be $\sim16.4 \mu\text{G}$. We also estimate the equipartition field to be $\sim235 \mu\text{G}$ with a minimum energy of $E_{\min}=6.3\times10^{48} \text{ erg}$.

When comparing N 103B with other similar type Ia SNRs we suggest that the SD types could be somewhat asymmetrical in appearance while DD are well and circularly shaped.

Acknowledgements The Australian Compact Array is part of the Australian Telescope which is funded by the Commonwealth of Australia for operation as National Facility managed by CSIRO. This paper includes archived data obtained through the Australia Telescope Online Archive (<http://atoa.atnf.csiro.au>). We used the KARMA and MIRIAD software packages developed by the ATNF.

References

- Alsaberi, R.Z.E., Maitra, C., Filipović, M.D., Bozzetto, L.M., Haberl, F., Maggi, P., Sasaki, M., Manjolović, P., Velović, V., Kavanagh, P., Maxted, N.I., Urošević, D., Rowell, G.P., Wong, G.F., For, B.-Q., O'Brien, A.N., Galvin, T.J., Staveley-Smith, L., Norris, R.P., Jarrett, T., Kothes, R., Luken, K.J., Hurley-Walker, N., Sano, H., Onić, D., Dai, S., Pannuti, T.G., Tothill, N.F.H., Crawford, E.J., Yew, M., Bojičić, I., Dénes, H., McClure-Griffiths, N., Gurovich, S., Fukui, Y.: Mon. Not. R. Astron. Soc. **486**(2), 2507 (2019). 1903.03226. doi:10.1093/mnras/stz971
- Anderson, M.C., Rudnick, L.: Astrophys. J. **456**, 234 (1996). doi:10.1086/176644
- Arbutina, B., Urošević, D., Andjelić, M.M., Pavlović, M.Z., Vukotić, B.: The Astrophysical Journal **746**(1), 79 (2012). doi:10.1088/0004-637X/746/1/79
- Arbutina, B., Urošević, D., Andjelić, M.M., Pavlović, M.Z., Vukotić, B.: Astrophys. J. **746**, 79 (2012). 1111.5465. doi:10.1088/0004-637X/746/1/79
- Arbutina, B., Urošević, D., Vučetić, M.M., Pavlović, M.Z., Vukotić, B.: Astrophys. J. **777**, 31 (2013). 1308.6110. doi:10.1088/0004-637X/777/1/31
- Axford, W.I., Leer, E., Skadron, G.: International Cosmic Ray Conference **11**, 132 (1977)
- Bell, A.R.: Mon. Not. R. Astron. Soc. **182**, 147 (1978). doi:10.1093/mnras/182.2.147
- Bell, A.R., Matthews, J.H., Blundell, K.M.: Mon. Not. R. Astron. Soc. **488**(2), 2466 (2019). 1906.12240. doi:10.1093/mnras/sty2466
- Bell, A.R., Schure, K.M., Reville, B.: Mon. Not. R. Astron. Soc. **418**, 1208 (2011). 1108.0582. doi:10.1111/j.1365-2966.2011.19571.x
- Blair, W.P., Ghavamian, P., Long, K.S., Williams, B.J., Borkowski, K.J., Reynolds, S.P., Sankrit, R.: Astrophys. J. **662**, 998 (2007). astro-ph/0703660. doi:10.1086/518414
- Blandford, R.D., Ostriker, J.P.: Astrophys. J. Lett. **221**, 29 (1978). doi:10.1086/182658
- Bojičić, I.S., Filipović, M.D., Parker, Q.A., Payne, J.L., Jones, P.A., Reid, W., Kawamura, A., Fukui, Y.: Mon. Not. R. Astron. Soc. **378**, 1237 (2007). astro-ph/0703727. doi:10.1111/j.1365-2966.2007.11784.x
- Borkowski, K.J., Reynolds, S.P., Hwang, U., Green, D.A., Petre, R., Krishnamurthy, K., Willett, R.: Astrophys. J. Lett. **771**, 9 (2013). 1305.7399. doi:10.1088/2041-8205/771/1/L9
- Borkowski, K.J., Williams, B.J., Reynolds, S.P., Blair, W.P., Ghavamian, P., Sankrit, R., Hendrick, S.P., Long, K.S., Raymond, J.C., Smith, R.C., Points, S., Winkler, P.F.: The Astrophysical Journal Letters **642**(2), 141 (2006)
- Bozzetto, L.M., Filipović, M.D.: Astrophys. Space Sci. **351**, 207 (2014). 1401.8025. doi:10.1007/s10509-014-1825-y
- Bozzetto, L.M., Filipovic, M.D., Crawford, E.J., Bojicic, I.S., Payne, J.L., Medik, A., Wardlaw, B., de Horta, A.Y.: Serbian Astronomical Journal **181**, 43 (2010). 1009.2816. doi:10.2298/SAJ1081043B
- Bozzetto, L.M., Filipovic, M.D., Crawford, E.J., De Horta, A.Y., Stupar, M.: Serbian Astronomical Journal **184**, 69 (2012a). 1205.1259. doi:10.2298/SAJ1284069B
- Bozzetto, L.M., Filipović, M.D., Crawford, E.J., Haberl, F., Sasaki, M., Urošević, D., Pietsch, W., Payne, J.L., de Horta, A.Y., Stupar, M., Tothill, N.F.H., Dickel, J., Chu, Y.-H., Gruendl, R.: Mon. Not. R. Astron. Soc. **420**, 2588 (2012b). 1111.6649. doi:10.1111/j.1365-2966.2011.20231.x
- Bozzetto, L.M., Filipovic, M.D., Crawford, E.J., Payne, J.L., de Horta, A.Y., Stupar, M.: Rev. Mexicana Astron. Astrofis. **48**, 41 (2012c). 1109.3945
- Bozzetto, L.M., Filipovic, M.D., Urosevic, D., Crawford, E.J.: Serbian Astronomical Journal **185**, 25 (2012d). 1211.1744. doi:10.2298/SAJ1285025B
- Bozzetto, L.M., Filipović, M.D., Crawford, E.J., Sasaki, M., Maggi, P., Haberl, F., Urošević, D., Payne, J.L., De Horta, A.Y., Stupar, M., Gruendl, R., Dickel, J.: Mon. Not. R. Astron. Soc. **432**, 2177 (2013). 1304.0495. doi:10.1093/mnras/stt568
- Bozzetto, L.M., Kavanagh, P.J., Maggi, P., Filipović, M.D., Stupar, M., Parker, Q.A., Reid, W.A., Sasaki, M., Haberl, F., Urošević, D., Dickel, J., Sturm, R., Williams, R., Ehle, M., Gruendl, R., Chu, Y.-H., Points, S., Crawford, E.J.: Mon. Not. R. Astron. Soc. **439**, 1110 (2014a). 1401.1868. doi:10.1093/mnras/stu051
- Bozzetto, L.M., Filipović, M.D., Urošević, D., Kothes, R., Crawford, E.J.: Mon. Not. R. Astron. Soc. **440**, 3220 (2014b). 1312.3706. doi:10.1093/mnras/stu499
- Bozzetto, L.M., Filipović, M.D., Vukotić, B., Pavlović, M.Z., Urošević, D., Kavanagh, P.J., Arbutina, B., Maggi, P., Sasaki, M., Haberl, F., Crawford, E.J., Roper, Q., mnras/stu1805, Points, S.D.: Astrophys. J. Suppl. Ser. **230**, 2 (2017). 1703.02676. doi:10.3847/1538-4365/aa653c
- Bozzetto, L.M., Filipovic, M.D., Haberl, F., Sasaki, M., Kavanagh, P., Maggi, P., Urosevic, D., Sturm, R.: Publication of Korean Astronomical Society **30**, 149 (2015). doi:10.5303/PKAS.2015.30.2.149
- Brantseg, T., McEntaffer, R.L., Bozzetto, L.M., Filipovic, M., Grieves, N.: Astrophys. J. **780**, 50 (2014). 1312.4790. doi:10.1088/0004-637X/780/1/50
- Cajko, K.O., Crawford, E.J., Filipovic, M.D.: Serbian Astronomical Journal **179**, 55 (2009). 0909.0310. doi:10.2298/SAJ0979055C
- Caprioli, D., Zhang, H., Spitkovsky, A.: Journal of Plasma Physics **84**(3), 715840301 (2018). 1801.01510. doi:10.1017/S0022377818000478
- Chakrabarti, S., Childs, F., Soderberg, A.: Astrophys. J. **819**, 37 (2016). 1510.08851. doi:10.3847/0004-637X/819/1/37
- Chu, Y.-H., Kennicutt, R.C. Jr.: Astron. J. **96**, 1874 (1988). doi:10.1086/114934
- Clarke, T.E.: Journal of Korean Astronomical Society **37**, 337 (2004). astro-ph/0412268. doi:10.5303/JKAS.2004.37.5.337
- Crawford, E.J., Filipovic, M.D., de Horta, A.Y., Stootman, F.H., Payne, J.L.: Serbian Astronomical Journal **177**, 61 (2008). doi:10.2298/SAJ0877061C
- Crawford, E.J., Filipović, M.D., Haberl, F., Pietsch, W., Payne, J.L., de Horta, A.Y.: Astron. Astrophys. **518**, 35 (2010). 1006.0287. doi:10.1051/0004-6361/201014767
- Crawford, E.J., Filipović, M.D., McEntaffer, R.L., Brantseg, T., Heitritter, K., Roper, Q., Haberl, F., Urošević, D.: Astron. J. **148**, 99 (2014). 1405.7788. doi:10.1088/0004-6256/148/5/99

- de Horta, A.Y., Filipović, M.D., Bozzetto, L.M., Maggi, P., Haberl, F., Crawford, E.J., Sasaki, M., Urošević, D., Pietsch, W., Gruendl, R., Dickel, J., Tothill, N.F.H., Chu, Y.-H., Payne, J.L., Collier, J.D.: *Astron. Astrophys.* **540**, 25 (2012). 1202.2618. doi:10.1051/0004-6361/201118694
- De Horta, A.Y., Sommer, E.R., Filipović, M.D., O'Brien, A., Bozzetto, L.M., Collier, J.D., Wong, G.F., Crawford, E.J., Tothill, N.F.H., Maggi, P., Haberl, F.: *Astron. J.* **147**, 162 (2014a). 1404.3823. doi:10.1088/0004-6256/147/6/162
- De Horta, A.Y., Filipovic, M.D., Crawford, E.J., Stootman, F.H., Pannuti, T.G., Bozzetto, L.M., Collier, J.D., Sommer, E.R., Kosakowski, A.R.: *Serbian Astronomical Journal* **189**, 41 (2014b). 0806.3605. doi:10.2298/SAJ140605001H
- De Looze, I., Barlow, M.J., Swinyard, B.M., Rho, J., Gomez, H.L., Matsuura, M., Wesson, R.: *Mon. Not. R. Astron. Soc.* **465**(3), 3309 (2017). 1611.00774. doi:10.1093/mnras/stw2837
- DeLaney, T., Koralesky, B., Rudnick, L., Dickel, J.R.: *Astrophys. J.* **580**, 914 (2002). astro-ph/0210355. doi:10.1086/343787
- Dickel, J.R., Milne, D.K.: *Astron. J.* **109**, 200 (1995). doi:10.1086/117266
- Dickel, J.R., van Breugel, W.J.M., Strom, R.G.: *Astron. J.* **101**, 2151 (1991). doi:10.1086/115837
- Douvion, T., Lagage, P.O., Cesarsky, C.J., Dwek, E.: *Astron. Astrophys.* **373**, 281 (2001). doi:10.1051/0004-6361:20010447
- Edwards, Z.I., Pagnotta, A., Schaefer, B.E.: *Astrophys. J.* **747**, 19 (2012). 1201.6377. doi:10.1088/2041-8205/747/2/L19
- Filipović, M.D., Haberl, F., Winkler, P.F., Pietsch, W., Payne, J.L., Crawford, E.J., de Horta, A.Y., Stootman, F.H., Reaser, B.E.: *Astron. Astrophys.* **485**, 63 (2008). 0805.0165. doi:10.1051/0004-6361:200809642
- For, B.-Q., Staveley-Smith, L., Hurley-Walker, N., Franzen, T., Kapińska, A.D., Filipović, M.D., Collier, J.D., Wu, C., Grieve, K., Callingham, J.R., Bell, M.E., Bernardi, G., Bowman, J.D., Briggs, F., Cappallo, R.J., Deshpande, A.A., Dwarakanath, K.S., Gaensler, B.M., Greenhill, L.J., Hancock, P., Hazelton, B.J., Hindson, L., Johnston-Hollitt, M., Kaplan, D.L., Lenc, E., Lonsdale, C.J., McKinley, B., McWhirter, S.R., Mitchell, D.A., Morales, M.F., Morgan, E., Morgan, J., Oberoi, D., Offringa, A., Ord, S.M., Prabu, T., Procopio, P., Shankar, N.U., Srivani, K.S., Subrahmanyam, R., Tingay, S.J., Wayth, R.B., Webster, R.L., Williams, A., Williams, C.L., Zheng, Q.: *Mon. Not. R. Astron. Soc.* **480**, 2743 (2018). doi:10.1093/mnras/sty1960
- Fryer, C.L., Ruiter, A.J., Belczynski, K., Brown, P.J., Bufano, F., Diehl, S., Fontes, C.J., Frey, L.H., Holland, S.T., Hungerford, A.L., Immeler, S., Mazzali, P., Meakin, C., Milne, P.A., Raskin, C., Timmes, F.X.: *Astrophys. J.* **725**, 296 (2010). 1007.0570. doi:10.1088/0004-637X/725/1/296
- Galvin, T.J., Filipovic, M.D.: *Serbian Astronomical Journal* **189**, 15 (2014). 1409.0591. doi:10.2298/SAJ140505002G
- Galvin, T.J., Filipovic, M.D., Crawford, E.J., Tothill, N.F.H., Wong, G.F., De Horta, A.Y.: *Serbian Astronomical Journal* **184**, 41 (2012). 1205.0066. doi:10.2298/SAJ1284041G
- Ghavamian, P., Seitenzahl, I.R., Vogt, F.P.A., Dopita, M.A., Terry, J.P., Williams, B.J., Winkler, P.F.: *Astrophys. J.* **847**, 122 (2017). 1705.03086. doi:10.3847/1538-4357/aa83b8
- Gooch, R.E.: *PASA* **14**, 106 (1997). doi:10.1071/AS97106
- Green, D.A.: *Bulletin of the Astronomical Society of India* **42**, 47 (2014). 1409.0637
- Grondin, M.-H., Sasaki, M., Haberl, F., Pietsch, W., Crawford, E.J., Filipović, M.D., Bozzetto, L.M., Points, S., Smith, R.C.: *Astron. Astrophys.* **539**, 15 (2012). 1201.1082. doi:10.1051/0004-6361/201117881
- Haberl, F., Filipović, M.D., Bozzetto, L.M., Crawford, E.J., Points, S.D., Pietsch, W., De Horta, A.Y., Tothill, N., Payne, J.L., Sasaki, M.: *Astron. Astrophys.* **543**, 154 (2012). 1206.5679. doi:10.1051/0004-6361/201218971
- Hachisu, I., Kato, M., Nomoto, K.: *Astrophys. J.* **470**, 97 (1996). doi:10.1086/310303
- Hughes, J.P., Hayashi, I., Helfand, D., Hwang, U., Itoh, M., Kirshner, R., Koyama, K., Markert, T., Tsunemi, H., Woo, J.: *Astrophys. J. Lett.* **444**, 81 (1995). doi:10.1086/187865
- Hughes, J.P.: *The Astrophysical Journal Letters* **545**(1), 53 (2000)
- Jones, T.J., Rudnick, L., DeLaney, T., Bowden, J.: *Astrophys. J.* **587**(1), 227 (2003). astro-ph/0212544. doi:10.1086/368149
- Joseph, T.D., Filipović, M.D., Crawford, E.J., Bojićić, I., Alexander, E.L., Wong, G.F., Andernach, H., Levernenz, H., Norris, R.P., Alsaberi, R.Z.E., Anderson, C., Barnes, L.A., Bozzetto, L.M., Bufano, F., Bunton, J.D., Cavallaro, F., Collier, J.D., Dénes, H., Fukui, Y., Galvin, T., Haberl, F., Ingallinera, A., Kapinska, A.D., Koribalski, B.S., Kothes, R., Li, D., Maggi, P., Maitra, C., Manojlović, P., Marvil, J., Maxted, N.I., O'Brien, A.N., Oliveira, J.M., Pennock, C.M., Raggi, S., Rowell, G., Rudnick, L., Sano, H., Sasaki, M., Seymour, N., Soria, R., Stupar, M., Tothill, N.F.H., Trigilio, C., Tsuge, K., Umana, G., Urošević, D., van Loon, J.T., Vardoulaki, E., Velović, V., Yew, M., Leahy, D., Chu, Y.-H., Michałowski, M.J., Kavanagh, P.J., Grieve, K.R.: *Mon. Not. R. Astron. Soc.*, 2277 (2019). 1909.10425. doi:10.1093/mnras/stz2650
- Katz-Stone, D.M., Kassim, N.E., Lazio, T.J.W., O'Donnell, R.: *Astrophys. J.* **529**, 453 (2000). doi:10.1086/308251
- Kavanagh, P.J., Sasaki, M., Points, S.D., Filipović, M.D., Maggi, P., Bozzetto, L.M., Crawford, E.J., Haberl, F., Pietsch, W.: *Astron. Astrophys.* **549**, 99 (2013). 1211.4746. doi:10.1051/0004-6361/201220431
- Kavanagh, P.J., Sasaki, M., Bozzetto, L.M., Points, S.D., Filipović, M.D., Maggi, P., Haberl, F., Crawford, E.J.: *Astron. Astrophys.* **583**, 121 (2015a). 1509.06475. doi:10.1051/0004-6361/201526987
- Kavanagh, P.J., Sasaki, M., Whelan, E.T., Maggi, P., Haberl, F., Bozzetto, L.M., Filipović, M.D., Crawford, E.J.: *Astron. Astrophys.* **579**, 63 (2015b). 1505.06458. doi:10.1051/0004-6361/201526143
- Kavanagh, P.J., Sasaki, M., Bozzetto, L.M., Filipović, M.D., Points, S.D., Maggi, P., Haberl, F.: *Astron. Astrophys.* **573**, 73 (2015c). 1409.6547. doi:10.1051/0004-6361/201424354

- Kavanagh, P.J., Sasaki, M., Bozzetto, L.M., Points, S.D., Crawford, E.J., Dickel, J., Filipović, M.D., Haberl, F., Maggi, P., Whelan, E.T.: *Astron. Astrophys.* **586**, 4 (2016). 1510.08922. doi:10.1051/0004-6361/201527414
- Kavanagh, P.J., Vink, J., Sasaki, M., Chu, Y.-H., Filipović, M.D., Ohm, S., Haberl, F., Manojlović, P., Maggi, P.: *Astron. Astrophys.* **621**, 138 (2019). 1809.01095. doi:10.1051/0004-6361/201833659
- Kerzendorf, W.E., Strampelli, G., Shen, K.J., Schwab, J., Pakmor, R., Do, T., Buchner, J., Rest, A.: *Mon. Not. R. Astron. Soc.* **479**, 192 (2018). 1709.06566. doi:10.1093/mnras/sty1357
- Krymskii, G.F.: Akademii Nauk SSSR Doklady **234**, 1306 (1977)
- Lewis, K.T., Burrows, D.N., Hughes, J.P., Slane, P.O., Garmire, G.P., Nousek, J.A.: *Astrophys. J.* **582**, 770 (2003). astro-ph/0209280. doi:10.1086/344717
- Li, C.-J., Chu, Y.-H., Gruendl, R.A., Weisz, D., Pan, K.-C., Points, S.D., Ricker, P.M., Smith, R.C., Walter, F.M.: *Astrophys. J.* **836**, 85 (2017). 1701.05852. doi:10.3847/1538-4357/836/1/85
- Lopez, L.A., Ramirez-Ruiz, E., Huppenkothen, D., Badenes, C., Pooley, D.A.: *Astrophys. J.* **732**, 114 (2011). 1011.0731. doi:10.1088/0004-637X/732/2/114
- Macri, L.M., Stanek, K.Z., Bersier, D., Greenhill, L.J., Reid, M.J.: *Astrophys. J.* **652**, 1133 (2006). astro-ph/0608211. doi:10.1086/508530
- Maggi, P., Haberl, F., Kavanagh, P.J., Sasaki, M., Bozzetto, L.M., Filipović, M.D., Vasilopoulos, G., Pietsch, W., Points, S.D., Chu, Y.-H., Dickel, J., Ehle, M., Williams, R., Greiner, J.: *Astron. Astrophys.* **585**, 162 (2016). 1509.09223. doi:10.1051/0004-6361/201526932
- Maggi, P., Filipovic, M.D., Vukotic, B., Ballet, J., Haberl, F., Maitra, C., Kavanagh, P., Sasaki, M., Stupar, M.: arXiv e-prints, 1908 (2019). 1908.11234
- Maitra, C., Haberl, F., Filipovic, M.D., Udalski, A., Kavanagh, P.J., Carpano, S., Maggi, P., Sasaki, M., Norris, R.P., O'Brien, A., Hotan, A., Szymanski, E.L.M.K., Soszynski, I., Poleski, R., Ulaczyk, K., Pietrukowicz, P., Kozłowski, S., Skowron, J., Mroz, P., Rybicki, K., Iwanek, P., Wrona, M.: arXiv e-prints, 1910 (2019). 1910.02792
- Markwardt, C.B.: In: Bohlander, D.A., Durand, D., Dowler, P. (eds.) *Astronomical Data Analysis Software and Systems XVIII*. Astronomical Society of the Pacific Conference Series, vol. 411, p. 251 (2009). 0902.2850
- Maxted, N.I., Filipović, M.D., Sano, H., Allen, G.E., Pannuti, T.G., Rowell, G.P., Grech, A., Roper, Q., Wong, G.F., Galvin, T.J., Fukui, Y., Collier, J.D., Crawford, E.J., Grieve, K., Horta, A.D., Manojlović, P., O'Brien, A.: *Astrophys. J.* **866**, 76 (2018). 1809.02249. doi:10.3847/1538-4357/aae082
- Meng, X., Li, J.: *Mon. Not. R. Astron. Soc.* **482**, 5651 (2019). 1811.11351. doi:10.1093/mnras/sty3092
- Nomoto, K., Kondo, Y.: *Astrophys. J. Lett.* **367**, 19 (1991). doi:10.1086/185922
- Nuza, S.E., Scannapieco, C., Chiappini, C., Junqueira, T.C., Minchev, I., Martig, M.: *Mon. Not. R. Astron. Soc.* **482**, 3089 (2019). 1805.06428. doi:10.1093/mnras/sty2882
- Onić, D., Urošević, D.: *Astrophys. J.* **805**, 119 (2015). 1503.08313. doi:10.1088/0004-637X/805/2/119
- Patnaude, D.J., Badenes, C., Park, S., Laming, J.M.: *Astrophys. J.* **756**, 6 (2012). 1206.6799. doi:10.1088/0004-637X/756/1/6
- Pavlović, M.Z.: *Mon. Not. R. Astron. Soc.* **468**, 1616 (2017). 1702.07418. doi:10.1093/mnras/stx497
- Pavlović, M.Z., Urošević, D., Vukotić, B., Arbutina, B., Göker, Ü.D.: *Astrophys. J. Suppl. Ser.* **204**, 4 (2013). 1210.4602. doi:10.1088/0067-0049/204/1/4
- Pavlović, M.Z., Urošević, D., Arbutina, B., Orlando, S., Maxted, N., Filipović, M.D.: *Astrophys. J.* **852**, 84 (2018). 1711.06013. doi:10.3847/1538-4357/aaale6
- Perlmutter, S., Aldering, G., Goldhaber, G., Knop, R.A., Nugent, P., Castro, P.G., Deustua, S., Fabbro, S., Goobar, A., Groom, D.E., Hook, I.M., Kim, A.G., Kim, M.Y., Lee, J.C., Nunes, N.J., Pain, R., Pennypacker, C.R., Quimby, R., Lidman, C., Ellis, R.S., Irwin, M., McMahon, R.G., Ruiz-Lapuente, P., Walton, N., Schaefer, B., Boyle, B.J., Filippenko, A.V., Matheson, T., Fruchter, A.S., Panagia, N., Newberg, H.J.M., Couch, W.J., Project, T.S.C.: *Astrophys. J.* **517**, 565 (1999). astro-ph/9812133. doi:10.1086/307221
- Pietrzyński, G., Graczyk, D., Gallenne, A., Gieren, W., Thompson, I.B., Pilecki, B., Karczmarek, P., Górska, M., Suchomska, K., Taormina, M., Zgirski, B., Wielgórski, P., Kołaczkowski, Z., Konorski, P., Villanova, S., Nardetto, N., Kervella, P., Bresolin, F., Kudritzki, R.P., Storm, J., Smolec, R., Narloch, W.: *Nature* **567**(7747), 200 (2019). 1903.08096. doi:10.1038/s41586-019-0999-4
- Reid, W.A., Stupar, M., Bozzetto, L.M., Parker, Q.A., Filipović, M.D.: *Mon. Not. R. Astron. Soc.* **454**, 991 (2015). 1508.06323. doi:10.1093/mnras/stv1992
- Rest, A., Suntzeff, N.B., Olsen, K., Prieto, J.L., Smith, R.C., Welch, D.L., Becker, A., Bergmann, M., Clocchiatti, A., Cook, K., Garg, A., Huber, M., Miknaitis, G., Minniti, D., Nikolaev, S., Stubbs, C.: *Nature* **438**, 1132 (2005). astro-ph/0510738. doi:10.1038/nature04365
- Rest, A., Matheson, T., Blondin, S., Bergmann, M., Welch, D.L., Suntzeff, N.B., Smith, R.C., Olsen, K., Prieto, J.L., Garg, A., Challis, P., Stubbs, C., Hickern, M., Modjaz, M., Wood-Vasey, W.M., Zenteno, A., Damke, G., Newman, A., Huber, M., Cook, K.H., Nikolaev, S., Becker, A.C., Miceli, A., Covarrubias, R., Morelli, L., Pignata, G., Clocchiatti, A., Minniti, D., Foley, R.J.: *Astrophys. J.* **680**, 1137 (2008). 0801.4762. doi:10.1086/587158
- Reynolds, S.P., Ellison, D.C.: *Astrophys. J. Lett.* **399**, 75 (1992). doi:10.1086/186610
- Reynolds, S.P., Borkowski, K.J., Hwang, U., Hughes, J.P., Badenes, C., Laming, J.M., Blondin, J.M.: *Astrophys. J.* **668**, 135 (2007). 0708.3858. doi:10.1086/522830
- Reynolds, S.P., Borkowski, K.J., Green, D.A., Hwang, U., Harrus, I., Petre, R.: *Astrophys. J.* **680**, 41 (2008). 0803.1487. doi:10.1086/589570
- Reynoso, E.M., Hughes, J.P., Moffett, D.A.: *Astron. J.* **145**, 104 (2013). 1302.4678. doi:10.1088/0004-6256/145/4/104

- Riess, A.G., Filippenko, A.V., Challis, P., Clocchiatti, A., Diercks, A., Garnavich, P.M., Gilliland, R.L., Hogan, C.J., Jha, S., Kirshner, R.P., Leibundgut, B., Phillips, M.M., Reiss, D., Schmidt, B.P., Schommer, R.A., Smith, R.C., Spyromilio, J., Stubbs, C., Suntzeff, N.B., Tonry, J.: *Astron. J.* **116**, 1009 (1998). [astro-ph/9805201](#). doi:10.1086/300499
- Roper, Q., McEntaffer, R.L., DeRoo, C., Filipović, M., Wong, G.F., Crawford, E.J.: *Astrophys. J.* **803**, 106 (2015). doi:10.1088/0004-637X/803/2/106
- Roper, Q., Filipović, M., Allen, G.E., Sano, H., Park, L., Pannuti, T.G., Sasaki, M., Haberl, F., Kavanagh, P.J., Yamane, Y., Yoshiike, S., Fujii, K., Fukui, Y., Seitenzahl, I.R.: *Mon. Not. R. Astron. Soc.* **479**, 1800 (2018). doi:10.1093/mnras/sty1196
- Sano, H., Yamane, Y., Tokuda, K., Fujii, K., Tsuge, K., Nagaya, T., Yoshiike, S., Filipović, M.D., Alsaberi, R.Z.E., Barnes, L., Onishi, T., Kawamura, A., Minamidani, T., Mizuno, N., Yamamoto, H., Tachihara, K., Maxted, N., Voisin, F., Rowell, G., Yamaguchi, H., Fukui, Y.: *Astrophys. J.* **867**(1), 7 (2018). 1806.10299. doi:10.3847/1538-4357/aae07c
- Sano, H., Matsumura, H., Nagaya, T., Yamane, Y., Alsaberi, R.Z.E., Filipović, M.D., Tachihara, K., Fujii, K., Tokuda, K., Tsuge, K., Yoshiike, S., Onishi, T., Kawamura, A., Minamidani, T., Mizuno, N., Yamamoto, H., Inutsuka, S., Inoue, T., Maxted, N., Rowell, G., Sasaki, M., Fukui, Y.: *Astrophys. J.* **873**, 40 (2019a). 1809.02481. doi:10.3847/1538-4357/ab02fd
- Sano, H., Matsumura, H., Yamane, Y., Maggi, P., Fujii, K., Tsuge, K., Tokuda, K., Alsaberi, R.Z.E., Filipović, M.D., Maxted, N., Rowell, G., Uchida, H., Tanaka, T., Muraoka, K., Takekoshi, T., Onishi, T., Kawamura, A., Minamidani, T., Mizuno, N., Yamamoto, H., Tachihara, K., Inoue, T., Inutsuka, S., Voisin, F., Tothill, N.F.H., Sasaki, M., McClure-Griffiths, N.M., Fukui, Y.: *Astrophys. J.* **881**(1), 85 (2019b). 1904.04836. doi:10.3847/1538-4357/ab2ade
- Sasaki, M., Haberl, F., Henze, M., Saeedi, S., Williams, B.F., Plucinsky, P.P., Hatzidimitriou, D., Karampelas, A., Sokolovsky, K.V., Breitschwerdt, D., de Avillez, M.A., Filipović, M.D., Galvin, T., Kavanagh, P.J., Long, K.S.: *Astron. Astrophys.* **620**, 28 (2018). 1809.08020. doi:10.1051/0004-6361/201833588
- Sault, R.J., Teuben, P.J., Wright, M.C.H.: In: Shaw, R.A., Payne, H.E., Hayes, J.J.E. (eds.) *Astronomical Data Analysis Software and Systems IV*. ASP Conference Series, vol. 77, p. 433 (1995). [arXiv:astro-ph/0612759](#)
- Schaefer, B.E., Pagnotta, A.: *Nature* **481**, 164 (2012). doi:10.1038/nature10692
- Someya, K., Bamba, A., Ishida, M.: *Publ. Astron. Soc. Jpn.* **66**, 26 (2014). 1310.4244. doi:10.1093/pasj/pst027
- Steidel, C.C., Erb, D.K., Shapley, A.E., Pettini, M., Reddy, N., Bogosavljević, M., Rudie, G.C., Rakic, O.: *Astrophys. J.* **717**, 289 (2010). 1003.0679. doi:10.1088/0004-637X/717/1/289
- Titus, N., Stappers, B.W., Morello, V., Caleb, M., Filipović, M.D., McBride, V.A., Ho, W.C.G., Buckley, D.A.H.: *Mon. Not. R. Astron. Soc.* **487**(3), 4332 (2019). 1906.04592. doi:10.1093/mnras/stz1578
- Tran, A., Williams, B.J., Petre, R., Ressler, S.M., Reynolds, S.P.: *Astrophys. J.* **812**, 101 (2015). 1509.00877. doi:10.1088/0004-637X/812/2/101
- Tsujimoto, T., Nomoto, K., Yoshii, Y., Hashimoto, M., Yanagida, S., Thielemann, F.-K.: *Mon. Not. R. Astron. Soc.* **277**, 945 (1995). doi:10.1093/mnras/277.3.945
- Urošević, D., Pavlović, M.Z., Arbutina, B.: *The Astrophysical Journal* **855**(1), 59 (2018). doi:10.3847/1538-4357/aaac2d
- Urošević, D.: *Astrophys. Space Sci.* **354**, 541 (2014). 1408.1107. doi:10.1007/s10509-014-2095-4
- van der Heyden, K.J., Behar, E., Vink, J., Rasmussen, A.P., Kaastra, J.S., Bleeker, J.A.M., Kahn, S.M., Mewe, R.: *Astron. Astrophys.* **392**, 955 (2002). doi:10.1051/0004-6361:20020963
- Vink, J.: In: Wilson, A. (ed.) *The X-ray Universe 2005*. ESA Special Publication, vol. 604, p. 319 (2006). [astro-ph/0601131](#)
- Warth, G., Sasaki, M., Kavanagh, P.J., Filipović, M.D., Points, S.D., Bozzetto, L.M.: *Astron. Astrophys.* **567**, 136 (2014). 1408.1850. doi:10.1051/0004-6361/201423575
- Williams, B.J., Borkowski, K.J., Reynolds, S.P., Ghavamian, P., Raymond, J.C., Long, K.S., Blair, W.P., Sankrit, R., Winkler, P.F., Hendrick, S.P.: *Astrophys. J.* **790**, 139 (2014). 1406.3031. doi:10.1088/0004-637X/790/2/139
- Williams, B.J., Borkowski, K.J., Reynolds, S.P., Ghavamian, P., Blair, W.P., Long, K.S., Sankrit, R.: *Astrophys. J.* **755**, 3 (2012). 1206.1054. doi:10.1088/0004-637X/755/1/3
- Williams, B.J., Borkowski, K.J., Reynolds, S.P., Ghavamian, P., Raymond, J.C., Long, K.S., Blair, W.P., Sankrit, R., Winkler, P.F., Hendrick, S.P.: In: AAS/High Energy Astrophysics Division, vol. 14, p. 120 (2014)
- Williams, B.J., Blair, W.P., Borkowski, K.J., Ghavamian, P., Hendrick, S.P., Long, K.S., Petre, R., Raymond, J.C., Rest, A., Reynolds, S.P., Sankrit, R., Seitenzahl, I.R., Winkler, P.F.: *The Astrophysical Journal Letters* **865**(2), 13 (2018)
- Winkler, P.F., Gupta, G., Long, K.S.: *The Astrophysical Journal* **585**(1), 324 (2003)
- Woods, T.E., Ghavamian, P., Badenes, C., Gilfanov, M.: *Nature Astronomy* **1**, 800 (2017). 1709.09190. doi:10.1038/s41550-017-0263-5
- Wright, M., Dickel, J., Koralesky, B., Rudnick, L.: *Astrophys. J.* **518**, 284 (1999). doi:10.1086/307270
- Yamaguchi, H., Badenes, C., Foster, A.R., Bravo, E., Williams, B.J., Maeda, K., Nobukawa, M., Eriksen, K.A., Brickhouse, N.S., Petre, R., Koyama, K.: *Astrophys. J.* **801**, 31 (2015). 1502.04255. doi:10.1088/2041-8205/801/2/L31
- Zanardo, G., Staveley-Smith, L., Ng, C.-Y., Gaensler, B.M., Potter, T.M., Manchester, R.N., Tzioumis, A.K.: *Astrophys. J.* **767**, 98 (2013). 1301.6527. doi:10.1088/0004-637X/767/2/98